Available online at www.CivileJournal.org

Civil Engineering Journal

(E-ISSN: 2476-3055; ISSN: 2676-6957)

Vol. 11, No. 04, April, 2025

Development of Novel Surrogate Models for Stress Concentration Factors in Composite Reinforced Tubular KT-Joints

Mohsin Iqbal [1*], Saravanan Karuppanan [1], Veeradasan Perumal [1], Mark Ovinis [2], Muhammad Iqbal [3]

[1] *Department of Mechanical Engineering, Universiti Teknologi PETRONAS, Seri Iskandar 32610, Malaysia.*

[2] *School of Engineering and the Built Environment, Birmingham City University, Birmingham, United Kingdom.*

[3] *Department of Mechanical Engineering, CECOS University of IT & Emerging Sciences, Phase-6 Hayatabad, Peshawar, Pakistan.*

Received 01 January 2025; Revised 08 March 2025; Accepted 14 March 2025; Published 01 April 2025

Abstract

Circular hollow section (CHS) joints are among the most critical components in offshore jackets, often requiring rehabilitation to maintain structural integrity. The structural stress approach, based on stress concentration factors (SCFs) for hot-spot stress (HSS) calculations, is commonly used to estimate the fatigue life of critical structural elements such as CHS joints. Various empirical models exist for the rapid estimation of SCF in composite-reinforced CHS joints; however, most studies focus on SCF at the crown and saddle positions under uniplanar loading. This limitation reduces their applicability to multi-planar loading conditions, potentially leading to the underestimation of HSS. This study investigates the use of fiber-reinforced polymer (FRP) composites to strengthen CHS KT-joints under complex loading, focusing on reducing SCF and improving fatigue life. A total of 5,429 finite element simulations were conducted to examine the effects of geometric and reinforcement parameters on SCF. The simulation data were used to train artificial neural networks (ANNs), which were incorporated into a computational tool for the rapid approximation of hot-spot stress in FRP-reinforced KT-joints. The application of composites to CHS joints significantly reduces SCF, particularly with an increased number of reinforcement layers, a higher elastic modulus, and an orthogonal fiber orientation to the weld toe. This study presents a novel methodology for developing efficient models to estimate SCF in composite-reinforced CHS joints under complex loading, addressing a key gap in fatigue design for such joints. The developed computational tool enables the rapid calculation of hot-spot stress in CHS joints.

Keywords: Circular Hollow Section Joints; Composite Reinforcement; Stress Concentration Factors (SCF); Artificial Neural Networks (ANN); Structural Rehabilitation; Surrogate Modelling.

1. Introduction

Tubular structures are extensively used in offshore jackets due to their high specific stiffness and low drag characteristics [1, 2]. The structural integrity of these structures primarily depends on the performance of their tubular joints, which are highly susceptible to fatigue damage due to stress concentration [3]. Various repair and strengthening techniques have been explored to enhance the durability of these joints, including internal and external ring stiffeners, gusset plates, collar plates, and mechanical clamps [4]. In recent years, fiber-reinforced polymer (FRP) composites have gained attention as a viable rehabilitation method due to their high strength-to-weight ratio, corrosion resistance, and ease of application [4, 5]. While composite reinforcement techniques have been acknowledged in ASME PCC-2 [6] and

* Corresponding author: mohsin_22005143@utp.edu.my

http://dx.doi.org/10.28991/CEJ-2025-011-04-012

ISO 24817 [7] as effective repair methods, their impact on stress concentration factors (SCFs) in tubular joints, a critical parameter in fatigue life assessment using the structural hot-spot stress (HSS) approach [8], remains insufficiently quantified, limiting their integration into structural design codes.

Several studies have investigated SCF reduction in CHS joints through composite reinforcement. The first article on this topic was published by Sadat Hosseini et al. [9] in 2019. Since then, within a relatively short period, various researchers have contributed to this field. These articles have been critically analyzed and listed in chronological order in Table 1. The primary focus has been on the numerical and experimental investigation of SCF reduction in various types of CHS joints (T/Y, K, X, TT, and KT joints) reinforced with composites. Most studies have examined a specific planar load type (axial compression, in-plane bending (IPB), or out-of-plane bending (OPB)) and have used simplified load configurations. While several studies target T/Y joints, fewer focus on more complex geometries such as KT and DKT joints. Given the identified research gap, it was essential to select a frequently encountered joint type, such as KT-joints, for investigation. Notably, KT-joints are among the most complex of the composite-reinforced joints studied.

Table 1. Literature on SCF in Composite-Reinforced CHS Joints in Chronological Order

S. No.	Reference	Joint type	Load type/direction
1	Sadat Hosseini et al. [9]	T/Y	IPB, OPB
2	Sadat Hosseini et al. [10]	T/Y	Axial compression, IPB, OPB
3	Tong et al. [11]	K	Balanced axial load
4	Xu et al. [12]	K	Balance axial load
5	Sadat Hosseini et al. [13]	T/Y	Axial compression
6	Nassirian et al. [14]	T/Y	Axial compression
7	Hosseini et al. [15]	T/Y	Axial compression
8	Nassiraei et al. [16]	T/Y	IPB
9	Nassiraei et al. [17]	T/Y	OPB
10	Sadat Hosseini et al. [18]	KT	Axial loads on all braces
11	Nassiraei et al. [19]	X	OPB
12	Nassiraei et al. [20]	X	OPB
13	Zavvar et al. [21]	KT	IPB, OPB on all braces
14	Nassiraei et al. [22]	X	Axial compression, IPB, OPB
15	Xu et al. [23]	TT	Axial tension
16	Mohamed et al. [24]	K	Balance axial load
17	Mohamed et al. [25]	T/Y	Axial compression
18	Sadat Hosseini et al. [26]	T/Y	IPB, OPB
19	Zavvar et al. [27]	DKT	Axial loads on all braces
20	Mohamed et al. [28]	T/Y	IPB, OPB
21	Rashnooie et al. [29]	T/Y	IPB
22	Zavvar et al. [30, 31]	DKT	Axial loads on all braces
23	Rezadoost et al. [32]	T/Y	OPB

Hosseini et al. [18] investigated KT-joints under three configurations of brace axial loading using 1,458 finite element (FE) simulations in ABAQUS. This study was the first to examine the composite reinforcement of KT-joints. A parametric study was also carried out, but the results were comparable to those of Sadat Hosseini et al. [9, 10, 13] for T/Y joints. It was reported that the SCF decreases with increasing brace inclination angle (θ) and increases with a rise in γ and τ. The effects of various configurations of glass fiber-reinforced polymer (GFRP) and carbon fiber-reinforced polymer (CFRP) reinforcement on SCF at specific positions of KT-joints were studied, and empirical models were developed. This study proposed thirty-eight parametric equations for determining SCF at the crown, saddle, heel, and toe of KT-joints subjected to axial loads on all braces.

Similarly, Zavvar et al. [21] investigated composite-reinforced KT-joints under bending loads. They simulated 2,920 FE models of composite-reinforced KT-joints under IPB and OPB in ABAQUS. Thirty-eight parametric equations were proposed for determining SCF at the crown, saddle, heel, and toe of KT-joints subjected to IPB or OPB loading on all braces. These parametric equations for determining SCF at the crown for IPB and at the saddle for OPB in composite-reinforced and unreinforced KT-joints represent a significant contribution. A sensitivity analysis was conducted for KT-joints under IPB and OPB. It was found that increased reinforcement thickness and elastic modulus significantly enhanced the effect of composite reinforcement when subjected to IPB. Similarly, the reinforcement effect was more pronounced for high β and γ, while the impact of τ depended on the type of loading. On the other hand, for KT-joints under OPB, the effect of reinforcement thickness and elastic modulus was similar, but the impact of β and τ was minimal. The brace inclination angle affected the SCF under IPB but had little influence under OPB.

When a joint is under multiaxial load, the location of maximum SCF, referred to here as peak HSS, can vary anywhere between crown and saddle positions, depending on the directions and magnitude of load components. Many practical load scenarios involve multiaxial loads (also referred to as multi-planar loads), for which the SCF (and HSS) and crown and saddle may not be sufficient for fatigue life estimation. Consequently, parametric models that can estimate the SCF in composite-reinforced joints are required for complex load situations. However, examining all available literature on CSF in composite-reinforced CHS joints, it was found that none of these joints have been investigated under combined load conditions. This essentially indicates that the optimal orientation and empirical models for combined-loaded joints remain unexplored.

When a joint is subjected to multiaxial loading, the location of the maximum SCF, referred to here as peak HSS, can vary anywhere between the crown and saddle positions, depending on the direction and magnitude of the load components [33]. Many practical load scenarios involve multiaxial loads (also referred to as multi-planar loads), for which SCF (and HSS) at the crown and saddle alone may not be sufficient for fatigue life estimation. Consequently, parametric models capable of estimating SCF in composite-reinforced joints under complex loading conditions are required. However, after reviewing all available literature on SCF in composite-reinforced CHS joints, it was found that none of these joints have been investigated under combined loading conditions. This highlights the fact that the optimal reinforcement orientation and empirical models for combined-loaded joints remain unexplored.

This study investigates an alternative MATLAB-based computational approach for GFRP-reinforced KT-joints. A surrogate modeling approach is employed, comprising finite element analysis (FEA) for data generation and artificial neural networks (ANNs) for developing predictive functions capable of rapidly estimating SCF/HSS. Unlike previous studies, which focused solely on the crown and saddle positions, this study examines SCF across the entire brace axis. Since SCF is typically higher at the central brace interface than at the inclined brace interface [34], only the chord-central brace interface is considered. Load is applied to the central brace of the joint [35]. Extensive FE simulations were conducted, generating approximately 1,465 models based on geometric parameters (β, γ, τ, θ, and ζ) and FRP reinforcement parameters (η and Ω). ANNs were used to develop empirical models for SCFs in both unreinforced and reinforced joints. The accuracy and effectiveness of the empirical models were rigorously validated through FEA and experimental testing.

This study investigates alternative MATLAB code/functions for GFRP-reinforced KT-joint. A surrogate approach comprising FEA for data generation and ANN for developing functions that can estimate SCF/HSS rapidly. Unlike previous studies, which focused solely on the crown and saddle position, this study investigates SCF all around the brace axis. Since SCF is usually higher at the central brace interface than the inclined brace interface braces, only the chord-central brace interface is considered. Load is applied on the central brace of the joint. Extensive finite element (FE) simulations were conducted, generating approximately 5,429 models based on geometric parameters $\beta, \gamma, \tau, \theta$ and ζ and FRP reinforcement parameters η and Ω. ANNs were used to develop surrogate models for SCFs in both unreinforced and reinforced joints. The accuracy and effectiveness of the empirical models were rigorously validated through FEA and experimental testing.

2. Methodology

This research is primarily based on numerical simulations using FEA, with the FE model validated through existing literature and experimental data. The KT-joint geometry was defined as a function of dimensionless parameters to simulate a wide range of designs and develop generalized empirical expressions. These parameters were based on those used in the literature to represent a wide range of design configurations [27]. These parameters are defined in Equations 1 to 7.

$$\beta = d/D \tag{1}$$

$$\gamma = D/2T \tag{2}$$

$$\tau = t/T \tag{3}$$

$$\alpha = 2L/D \tag{4}$$

$$\zeta = g/D \tag{5}$$

$$\eta = E_{frp}/E_{steel} \tag{6}$$

$$\Omega = t_{FRP}/T_{chord} \tag{7}$$

where D is chord diameter, d is brace diameter, T is thickness of chord wall, t is thickness of brace wall, L is length of chord, g is gap between braces at chord surface, E_{steel} is elastic modulus of steel (base joint), E_{frp} is elastic modulus of reinforcement, and t_{FRP} is thickness of reinforcement.

A typical uniplanar KT-joint consists of one chord and three braces. Loads are primarily transferred from the brace elements to the chord, and the chord transfers these loads to piles and foundations. The chord usually has a larger diameter and thickness than the braces. CHS elements with huge and tiny diameters are unusual for structural applications. As these structural members are generally fabricated through the cold rolling of sheets, large thicknesses can induce severe residual stress, which is unacceptable. At the same time, minimal thicknesses may require tight tolerances and can cause welding issues. The chord length should be more than four times the chord diameter to avoid the effect of end conditions [36]. Based on these practical considerations, the typical range of various parameters has been identified [36–41] and listed in Table 2.

Table 2. Range of parameters used to define composite reinforced KT-joint

Type of parameters	Parameters	Range	Reference / Source
Dimensionless Geometric Parameters	$\tau = t/T$	0.3–0.7	ARSEM [38]
	$\gamma = D/2T$	12–20	ARSEM [38]
	$\alpha = 2L/D$	5–40	Smedley & Fisher and API [37, 39]
	$\beta = d/D$	0.4–0.8	ARSEM [38]
	$\zeta = g/D$	0.25–0.5	Ahmadi (2019), Ahmadi & Lotfollahi-Yaghin (2013), and Ahmadi & Zavvar (2015) [41–43]
Geometric Parameters	Inclined brace angle, θ	30–75°	ARSEM [38]
	Gap between central and inclined brace, g	50-100 (mm)	Ahmadi (2019) [41]
	Brace thickness (all), t	3–10 (mm)	Manufacturing limit (assumption)
	Chord thickness, T	3–10 (mm)	Manufacturing limit (assumption)
	Chord length, L	1800–3000 (mm)	α_{max}, D_{max}, $\alpha_{min,}$ and D_{min}, and Moffat et al. [36]
	Brace diameter, d	80–320 (mm)	β_{max}, D_{min}, and D_{max}
	Chord diameter, D	200–400 (mm)	$D \geq 150$ [37], γ_{max} and T_{max}
Reinforcement Parameters	Steel (chord/brace) Young's modulus, E_{steel}	211 GPa	Zhang et al. [44]
	Young's modulus of FRP, E_{frp}	21–204 (GPa)	Minimum: GFRP [45], Max: BFRP [46]
	Thickness of FRP, t_{frp}	0–5 (mm)	Min = no. reinforcement, Max=assumed half of D_{max}
Dimensionless Reinforcement Parameters	$\Omega = E_{frp}/E_{steel}$	0.10–0.96	Derived based on E_{frp} *and* E_{steel}
	$\eta = t_{frp}/T$	0–0.8	Derived based on t_{frp} *and* T

A set of possible design configurations was developed based on the geometric and reinforcement parameters $D, d, T, t, \Theta, g, E_{frp}$ and t_{frp}. Ten equidistant values were assigned to each variable. These eight sets were used to derive all the possible design points. This initial dataset of 10^8 design points included configurations that exceeded the range specified for dimensionless design variables. This dataset was filtered based on the defined range of dimensionless parameters to exclude the out-of-range design points.

The obtained dataset was still large (3.51×10^8), and simulating all these datasets would have taken too much time; hence, it needed to be reduced for simulations. Additionally, the developed empirical models needed to be equally representative of the entire range and not biased toward design points concentrated at one end. The final dataset for simulating in ANSYS was chosen by defining a pre-set number of equidistant designs, namely the first, the last, and the remaining equidistant points in between. This ensures that a representative sample of the entire design space is selected for simulation. A MATLAB code was written for efficiency. A parametric model of the KT-joint was simulated for various sizes covering the defined range of all parameters. Simulation results were used to train an ANN and develop empirical equations. These models were also validated experimentally. This methodology is similar to Sadat Hosseini et al. [18] and Zavvar et al. [21], with different tools used and load configuration focused. This methodology is illustrated in Figure 1 and discussed in the following sections.

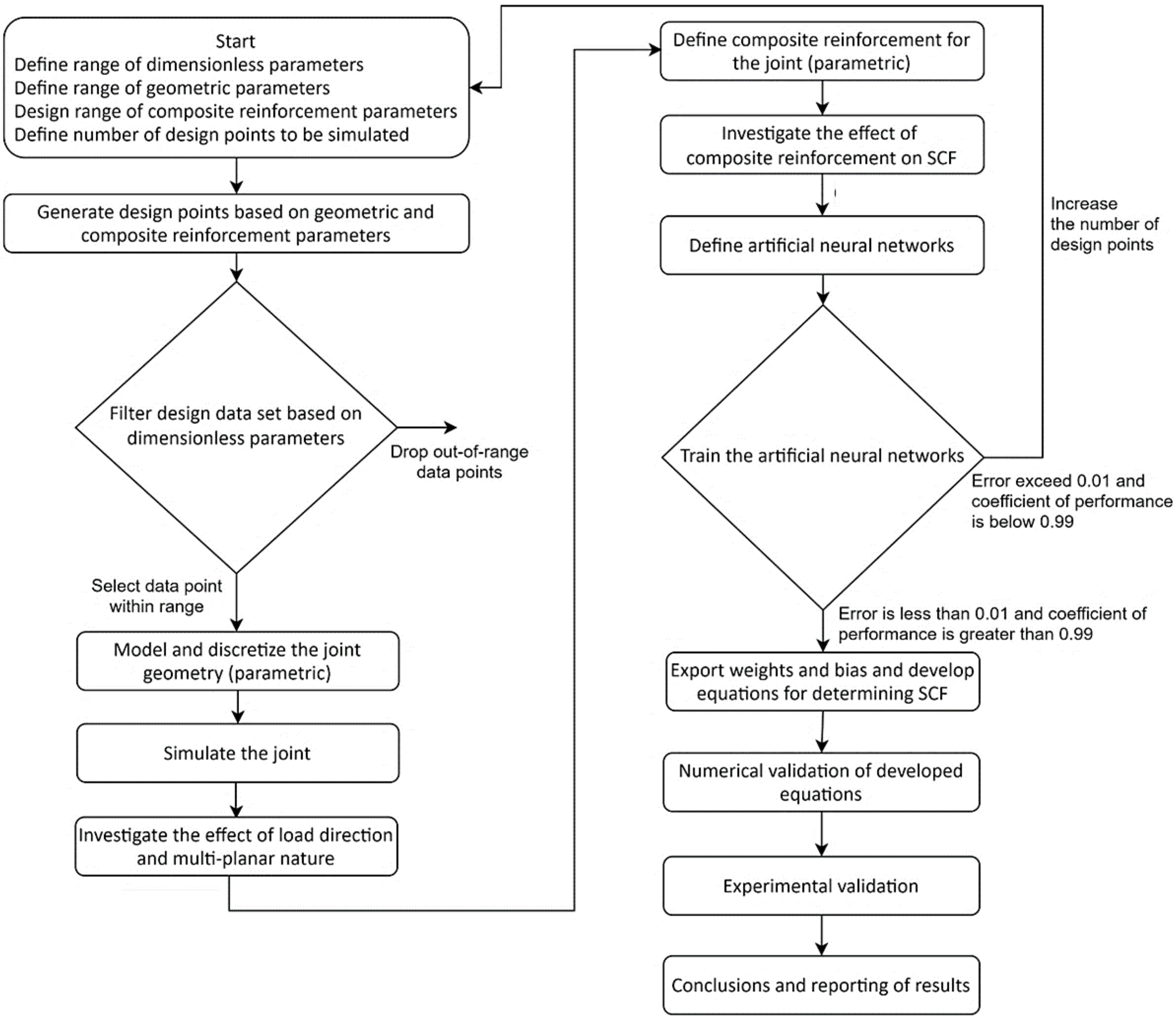

Figure 1. Methodology of investigating SCF in composite-reinforced CHS joints

2.1. Geometry Modeling

The geometry of a gapped KT-joint was modeled using the Design Modeler module of ANSYS Workbench. The geometry was defined as a function of geometric parameters D, T, d, t, Θ and L. These variables are depicted in Figure 2. All braces were assumed to have equal diameter and thickness, lying within the same plane. Additionally, the inclined braces were deemed symmetric to the orthogonal plane passing through the axis of the central brace.

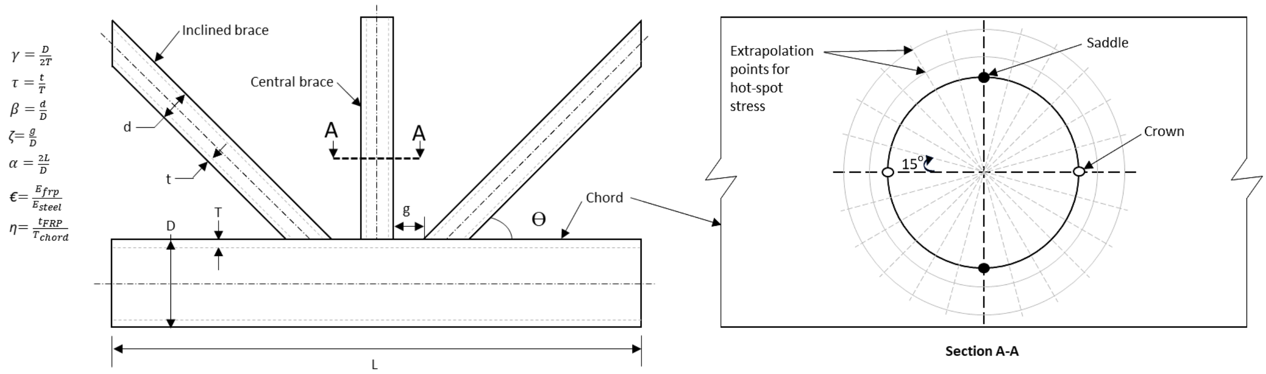

Figure 2. Circular hollow section KT-joint

The KT-joint was expressed as a function of dimensionless parameters commonly used in literature to ensure the generalizability of the developed empirical model across a broad spectrum of design configurations. A range was assigned to each input variable based on industry practices [47]. Various design points were generated, covering the entire range, and executed in MATLAB.

2.2. Meshing

Solid elements were used for meshing. The joint was divided into multiple sections and meshed with different mesh densities, ensuring a fine mesh at the interface region. The relative sizing was determined based on practical considerations, and then a scaling factor was incorporated into all sizing controls for mesh sensitivity analysis. Once a mesh-independent FE model was generated, it was optimized to reduce the computational time. A 10% reduction was applied to the control factor in each iteration, leading to the generation of a mesh with fewer elements and nodes. Subsequently, this new FE model was simulated, and the percentage difference in SCF for every 24 points along the weld toe was determined. Mesh independence was assessed by the difference in SCF, with a below 5% difference assumed acceptable.

Given the requirement to simulate various KT-joint designs in this study, ensuring that the mesh independence remains valid for the entire range was crucial. The validation process was repeated for three geometric designs, representing typical minimum, intermediate, and maximum sizes. Multiple FEM iterations were carried out, and sizing controls were established to generate a mesh-independent model throughout the range. These controls generate different numbers of elements depending on the size spectrum. Figure 3 shows the mesh independence for varied sizes of KT-joint, demonstrating the relationship between the mesh control factor (defined as a dividing factor for various sizing controls) and mesh sizes. Finally, a control factor of 0.8 was selected based on these plots. A typical KT-joint that has the dimensions as per the drawing given in Ahmadi & Zavvar [48], when meshed using these finalized controls, resulted in 223,630 elements, which is illustrated in Figure 4.

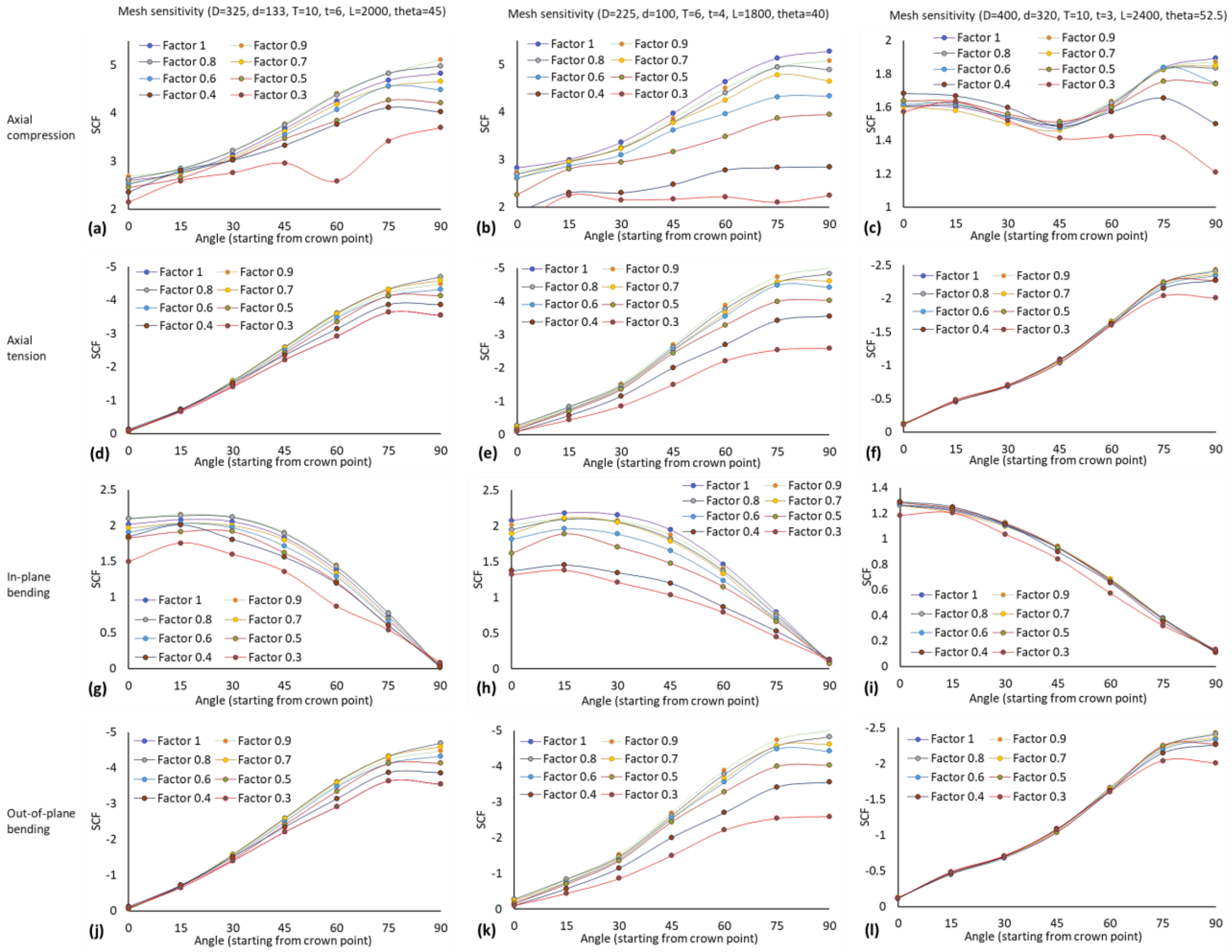

Figure 3. Mesh sensitivity analysis

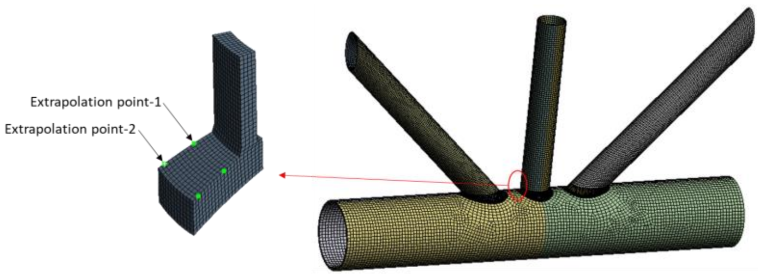

Figure 4. Meshed model

2.3. Validation of the Finite Element Model

The FE model of KT-joint was validated using the numerical and experimental results available in Ahmadi et al. [49]. The dimensions of KT-joint used for validation are shown in Figure 5-a. As illustrated in Figure 5-b, the maximum difference between the current and literature FE model is less than eight percent. However, a 15% difference was observed when compared to the experimental results from the literature, indicating potential undocumented details in the experimental setup. These omitted details likely contributed to a similar difference between the experimental model and the FE model of literature.

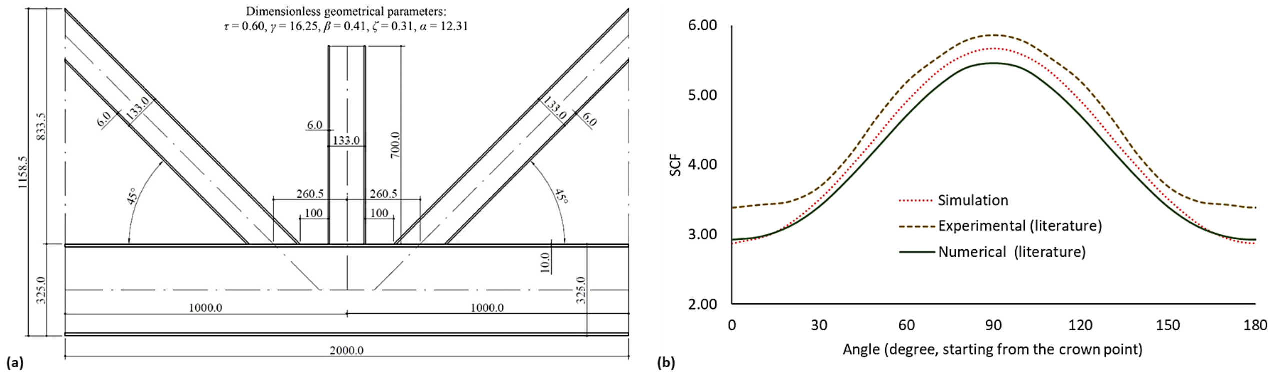

Figure 5. Validation of the numerical model with literature results: (a) geometry of the joint (b) SCF [48, 49]

To further validate the numerical model, experimental testing was conducted on a scaled-down KT-joint. The experimental setup is shown in Figure 6. Figure 7-a presents the geometric details of the joint tested, while Figure 7-b compares the experimental SCF with that determined from the numerical model for the joint. The difference between the numerical and experimental SCF was less than 5 percent, which is considered acceptable. The detailed procedure for SCF determination is explained in the following section.

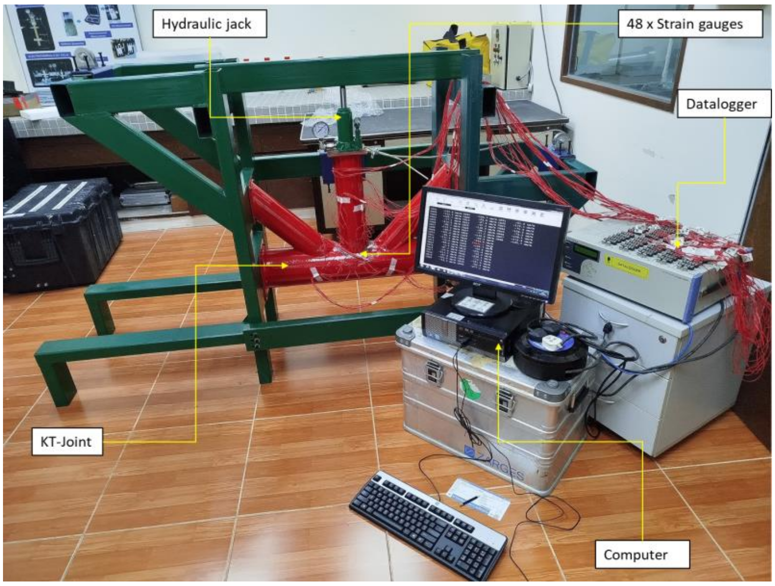

Figure 6. Experimental setup for testing KT-joint under axial compression load on the central brace

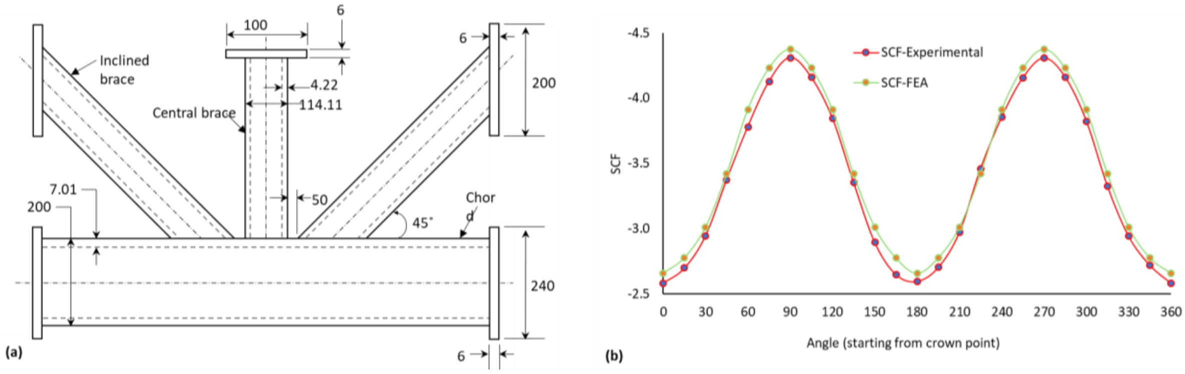

Figure 7. Experimental validation: (a) joint geometry (b) SCF

2.4. SCF Calculation

The commonly used nominal stress approach, covered in the structural design codes, e.g., IIW [50] and Eurocode [51], is simple; however, determining nominal stress for complex geometries is challenging for complex joints and loads [52]. Furthermore, this approach ignores the effect of geometric variation at the interface [52]. Local stress-based approaches have been developed and applied to address these limitations [50-54]. The concept that fatigue strength is related to stress or strain field near the weld toe was discovered in the 1960s [55]. This concept is used in the hot-spot stress (HSS) approach.

The HSS approach accounts for the factors causing stress concentration at the anticipated crack initiation site while excluding the local non-linear stress peak caused by the notch at the weld toe; thus, it avoids the shortcomings of the nominal stress approach and is computationally less demanding than other local stress approaches [52]. HSS considers the geometric dimensions of the joint and ignores the stress peak caused by the notch at the weld toe with the notch effect included in the experimental S-N curve. The exclusion of the notch effect is reasonable because the exact geometry of the weld may not be known at the design stage [52, 56].

The IIW recommendations for determining the HSS are based on the extrapolation of surface stress [56]. The reference points for extrapolations are selected as close as possible to the weld toe but outside the region affected by the weld toe singularity. IIW recommends distances of 0.4 and 1.0 times the chord thickness, T, from the weld toe [56]. SCF is determined using the HSS and nominal stress, as per Equation 8. The HSS is determined through linear extrapolation, as outlined in Equations 9 to 11 and illustrated in Figure 8.

$$SCF = \frac{HSS}{\sigma_{nominal}} \tag{8}$$

$$HSS = \sigma_1 + (\frac{\sigma_1 - \sigma_2}{\Delta_2})\Delta_1 \tag{9}$$

$$\Delta_1 = \sqrt{(x_1 - x)^2 + (y_1 - y)^2 + (z - z)^2} \tag{10}$$

$$\Delta_2 = \sqrt{(x_2 - x_1)^2 + (y_2 - y_1)^2 + (z_2 - z_1)^2} \tag{11}$$

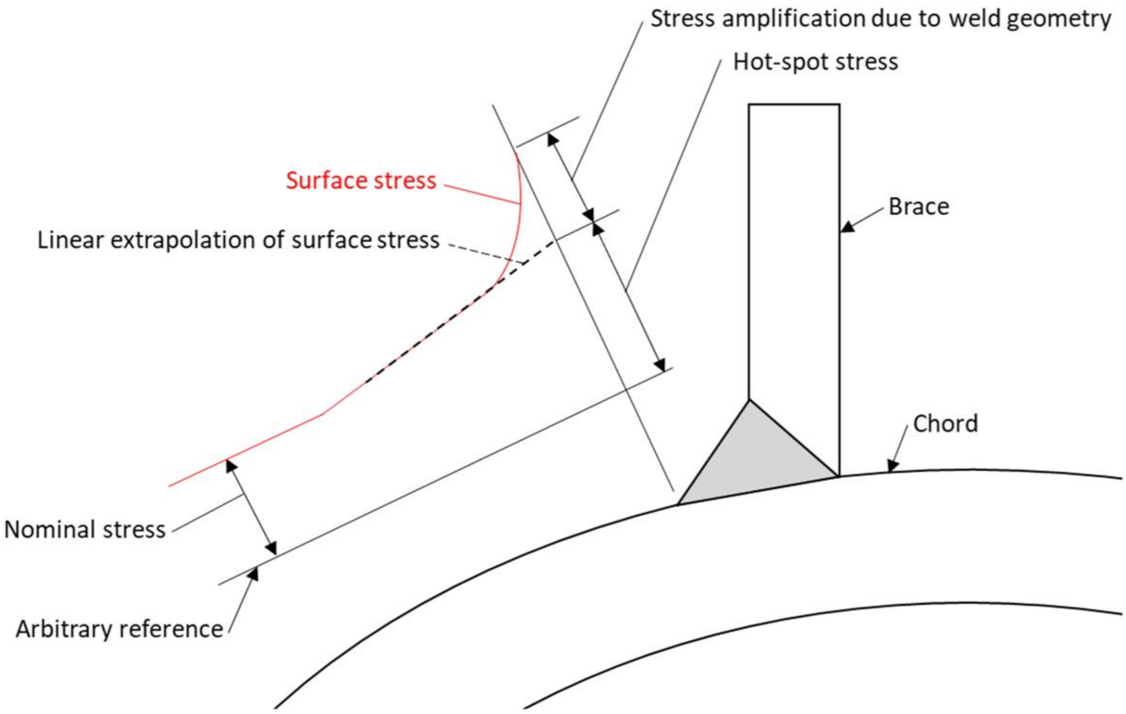

Figure 8. Hot-spot stress extrapolation at the weld toe [56, 57]

The HSS determined is utilized with the S-N curve for the fatigue life estimation. The stress magnitudes at reference points 1 (σ_1) and 2(σ_2) are crucial parameters in this determination, illustrated in Figure 8. Global coordinates (x, y, z),

(x_1, y_1, z_1) and (x_2, y_2, z_2) correspond to the weld notch and reference points, respectively. The position of these points is contingent upon the chord diameter, chord thickness, brace diameter, and brace thickness.

2.5. Composite Reinforcement

Composite reinforcement was used to strengthen the brace-chord interface. The reinforcement length has a negligible effect on SCF once a minimum length is reached [12]. The composite reinforcement was meshed with shell elements, as shown in Figure 4-b. The reinforcement layup was defined using ANSYS ACP (ANSYS Composite Pre/Post module). The joint and reinforcement material interface was assumed to be a perfect bond [13, 58]. Linear elastic steel properties were assigned to the joint, while the reinforcement material properties were defined as a variable. The FRP materials used for structural applications have orthotropic properties. Depending on the fiber architecture, FRP can be unidirectional, bidirectional, or tridirectional. It was found that unidirectional FRPs are the optimal choice for the reinforcement of tubular joints [12]. These simple yet structurally strongest unidirectional FRPs are the focus of this study.

Elastic modulus in fiber direction has the most prominent effect of SCF on the reinforced joint and can be used to decide the need for joint reinforcement [18, 21]. The ratio of elastic modulus of composite reinforcement material in the fiber direction to the base joint material was introduced as a parameter, Ω. The range of modulus ratio was selected to cover commonly used composite materials, given in Table 3.

Table 3. Mechanical properties of FRP materials [10, 59, 60]

Mechanical properties	BFRP	Glass/vinyl ester	Glass/ epoxy (Scotch ply 1002)	S-glass/ epoxy	Aramid/ epoxy (Kevlar 49/epoxy)	Carbon/ epoxy (T300-5208)	Carbon/ epoxy (AS/3501)	Boron/ epoxy
E_1(GPa)	17.8	28	38.6	43	76	132	138	204
E_1(GPa)	1.25	7	8.27	8.9	5.5	10.8	8.96	18.5
υ_{12}	0.15	0.29	0.26	0.27	0.34	0.24	0.3	0.23
G_{12}(GPa)	5.4	4.5	4.14	4.5	2.3	5.7	7.1	5.59
G_{13}(GPa)	5.4	4.5	4.14	3.18	2.3	5.7	7.1	-
G_{23}(GPa)	5.2	2.54	3.1	3.18	2.01	3.4	2.82	-

A second parameter was introduced to incorporate the amount of FRP materials used for reinforcement as the reinforcement thickness. If the inter-layer state of stress and strain are not considered, the total thickness can be modeled as a single layer to get a macroscopic response only. The unidirectional composite reinforcement was defined as a single layer and its thickness as a parameter. The upper limit for FRP reinforcement was defined as half of the maximum chord thickness, i.e., $T_{chord} = 10\ mm$, $T_{frp} = 5\ mm$. The thickness parameter was expressed as the ratio of FRP thickness to the chord thickness, denoted by η.

2.6. Loading and Boundary Conditions

The boundary conditions of chord ends range from pinned to fixed and can be considered as a fixed condition [61]. Both ends of the chord and inclined braces were fixed, with the load applied on the central brace of the tubular KT-joint, as illustrated in Figure 9. Linear elastic analysis was carried out, as recommended by N'Diaye et al. [62]. The SCF is independent of the magnitude of the applied load [33]; hence, any magnitude of load could be used. The applied load was chosen so that the material remains within the elastic limit [63]. A load of 30 MPa was used in axial load cases, which was determined using Equation 12. The bending load (IPB and OPB), equivalent to 30 MPa bending stress at the chord-brace interface, was applied and calculated using Equation 13.

$$\sigma_n = F/A \tag{12}$$

$$\sigma_b = 32dM/[d^4 - (d - 2t)^4] \tag{13}$$

where F is applied load (denoted as C for compression and T for tensile in Figure 9), A is cross-sectional area of the central brace, d is diameter of brace, M is bending moment (denoted as IPB and OPB in Figure 9), and t is thickness of brace.

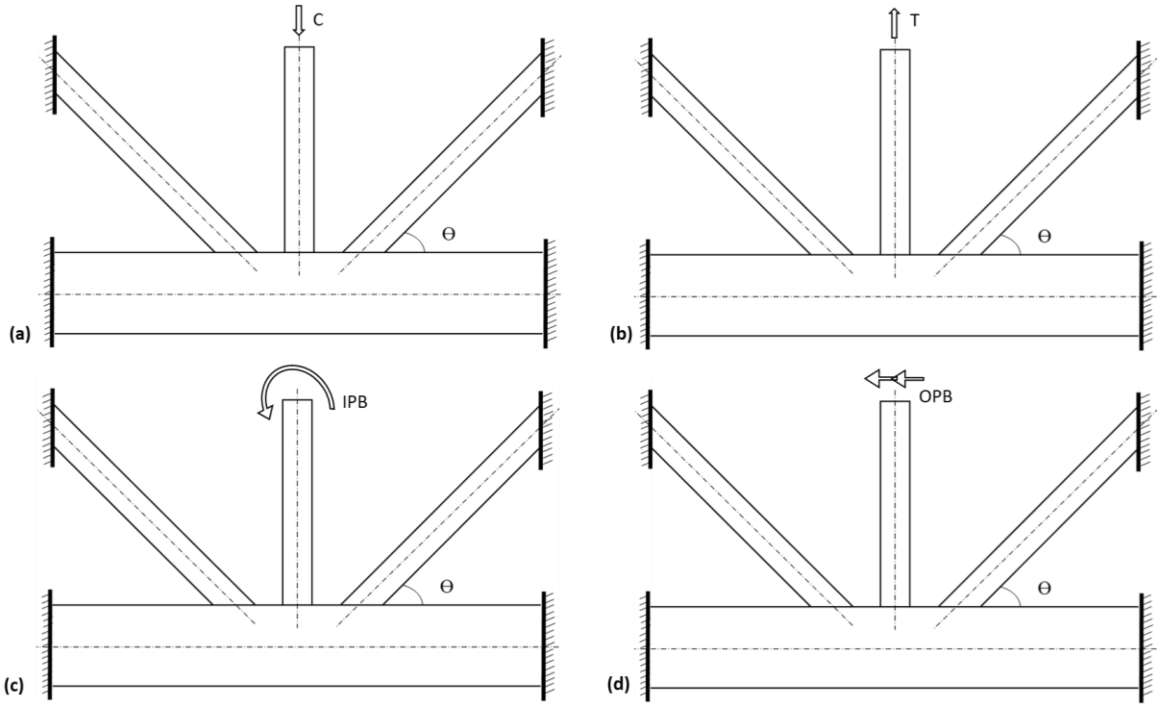

Figure 9. Loadings: (a) axial compression (b) axial tension (c) in-plane bending (iv) out-of-plane bending

2.7. Empirical Modeling of SCF using ANN

The conventional approach of experimental investigation has been replaced with simulations, notably FEA. However, FEA can be time-consuming and resource-intensive. Various empirical modeling techniques are employed to develop equations for tubular joints' rapid fatigue life estimation. It has been identified that ANN can offer greater accuracy than conventional approaches in developing such empirical models [64, 65]. This study used ANN to develop mathematical models for determining SCF in FRP-reinforced KT-joint. The ANN model was configured with dimensionless parameters defining the joint geometry, reinforcement as input, and SCF along the weld toe as output. A hidden layer with multiple neurons was defined between the input and output. The tangent-sigmoid transfer function was used to transfer the input to the hidden layer, and the linear transfer function was used for the hidden to the output layer. This model was trained using FEA data. A supervised learning algorithm, the "Levenger Marque algorithm ", was used to train ANN. This algorithm is particularly suitable for only a few thousand training points. The threshold limit for training was set as 0.01 for mean square error (MSE) and 0.999 for coefficient of determination (R^2). The weights and biases of the best epoch were used to express the trained function as a matrix equation. These developed functions and equations, combined with the principle of superposition, can be used to determine the SCF along the weld toe for any input joint parameters (Figure 10).

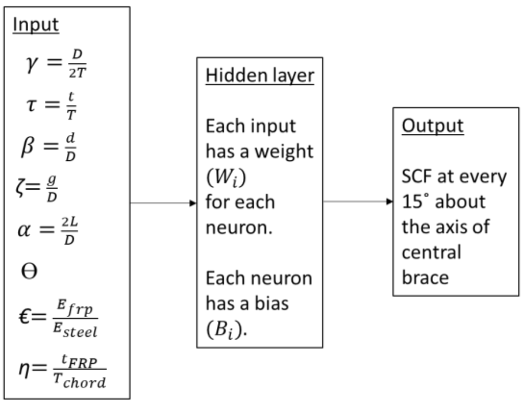

Figure 10. Black-box view of the developed ANN Architecture

3. Results and Discussion

KT-joints reinforced with various levels of the composite were simulated under axial, IPB, and OPB loads applied to the central brace. The SCF response around the weld was determined at every 15˚. The elastic modulus was incorporated into the developed models as the ratio of FRP modulus to steel modulus, while thickness was incorporated as the ratio of reinforcement thickness to chord thickness. Multiple combinations of orientations were evaluated, and the optimal orientation was found to be dependent on the applied load. Since the SCF is typically highest at the chord-central brace interface of the KT-joint, this area was specifically analyzed for the three planar load cases. The results showed that composite reinforcement significantly reduced the SCF and hot-spot stress (HSS). The elastic modulus in the fiber direction, thickness, and reinforcement orientation were the key parameters influencing this effect. A greater reinforcement thickness results in a higher reduction in SCF. Similarly, an increase in the elastic modulus of the reinforcement also leads to a greater reduction in SCF. The optimal reinforcement orientation varied based on the type of applied load. For an IPB load, the best orientation was along the chord axis, whereas for axial and OPB loads, the optimal direction was along the hoop direction of the chord, as shown in Figure 11. The axial load case exhibited quarter symmetry, whereas IPB and OPB demonstrated half symmetry.

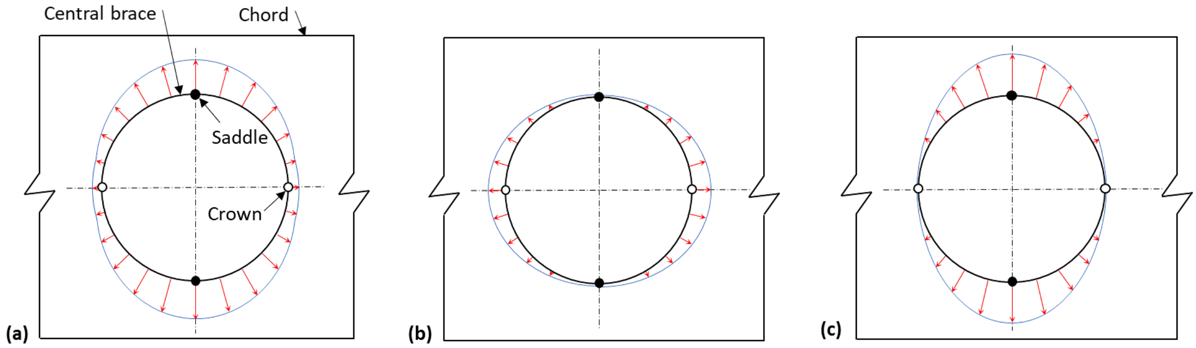

Figure 11. Effective direction of FRP for reduction of SCF: (a) Axial tension/compression (b) IPB (c) OPB [65]

For multi-planar loading, where the applied load has components in axial, IPB, and OPB directions, the optimum reinforcement direction depends on the load distribution. For a typical KT-joint subjected to OPB and axial loads on the central brace, the peak HSS always occurred at the saddle. However, when the joint was subjected to simultaneous bending and axial loads, both the peak HSS location and the optimum reinforcement orientation varied with the relative magnitudes of the load components. A detailed discussion on the optimal reinforcement orientation in CHS joints under complex loading conditions is provided in Iqbal et al. [65]. The peak HSS could be determined using the developed surrogate models and the principle of superposition. It was observed that the optimal reinforcement direction always remained orthogonal to the weld toe, but its orientation varied around the axis of the central brace depending on the applied load. The position of peak HSS dictated the optimal reinforcement orientation. Wrapping the reinforcement around the chord-central brace interface ensures that the FRP remains orthogonal to the weld toe, which maintains optimal reinforcement direction for any load and reduces the risk of reinforcement detachment from the joint. For zones away from the interface, the load is primarily axial (in the brace) or bending (in the chord). The optimum reinforcement direction in various zones, which offers the maximum SCF reduction for all load types (axial, IPB, and OPB), was applied in all simulations, as shown in Figure 12.

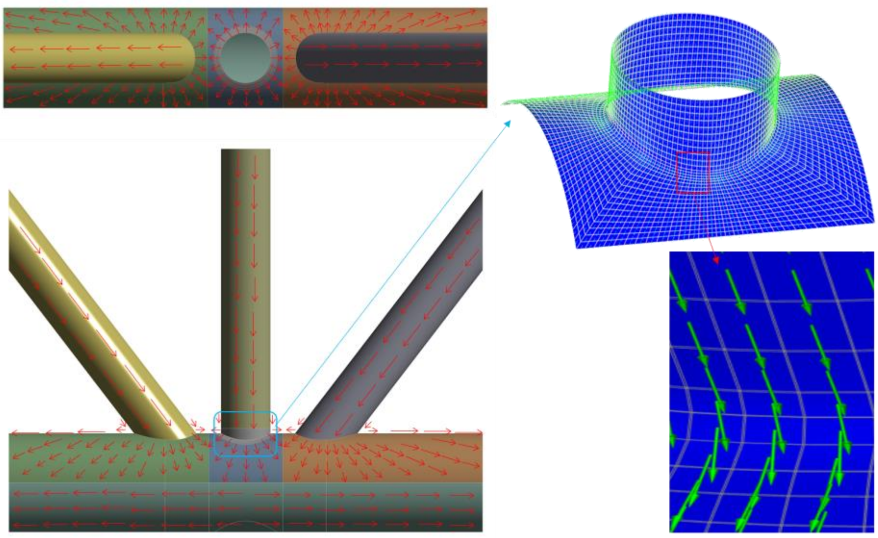

Figure 12. Reinforcement zones and orientation of unidirectional FRP

The FEA data, generated through 5,429 simulations, was used to develop empirical ANN-based models for predicting SCF in FRP-reinforced KT-joints subjected to any central brace load. These models take the ratio of FRP modulus to steel modulus and the ratio of FRP thickness to chord thickness as inputs, along with dimensionless geometric parameters. The models, in conjunction with the principle of superposition, enable the determination of HSS in FRP-reinforced joints subjected to complex loading conditions. The developed models were validated using detailed FEA for both uniplanar and multi-planar (complex) load cases. A typical KT-joint was modeled based on Ahmadi et al. [48] and simulated for validation. The unreinforced joint was labeled "1", while joints reinforced with composite thicknesses of 0.5, 1, 2, 3, 4, and 5 mm were labeled "2" to "7", respectively, in Figures 13 to 16. These joints were simulated using FEA and compared to SCF values predicted by the ANN-based surrogate models. The differences were 4.1%, 6.1%, 1.7%, and 8.0% for axial tensile, axial compressive, IPB, and OPB cases, respectively. These minor differences highlight the high accuracy of the developed models in SCF prediction.

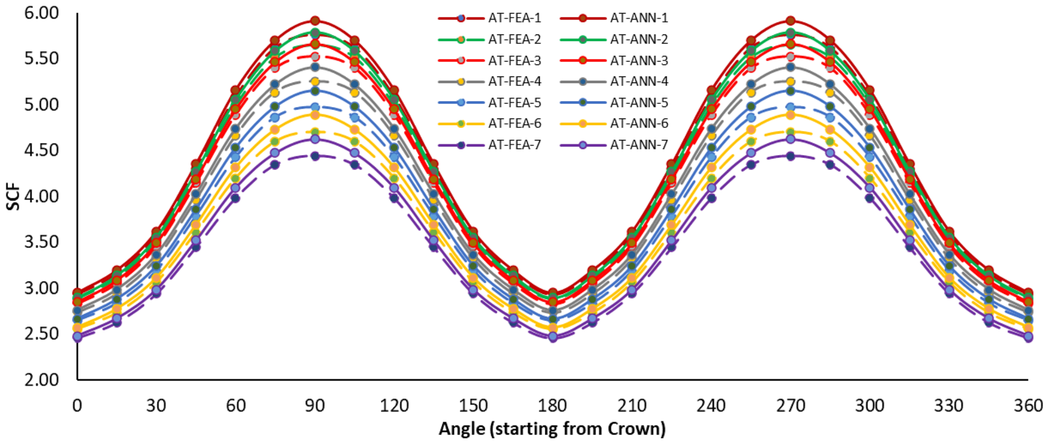

Figure 13. Comparison of SCF in KT-joint under axial tension

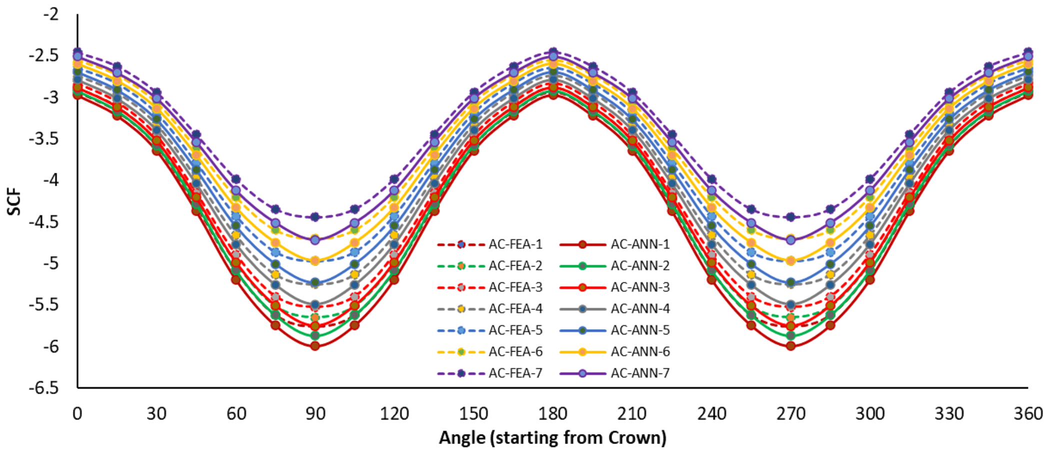

Figure 14. Comparison of SCF in KT-joint under axial compression

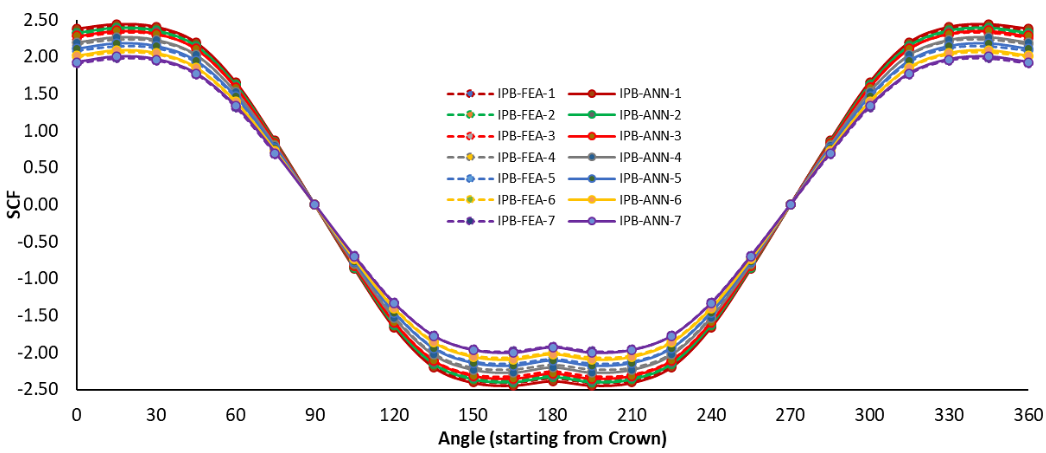

Figure 15. Comparison of SCF in KT-joint under IPB

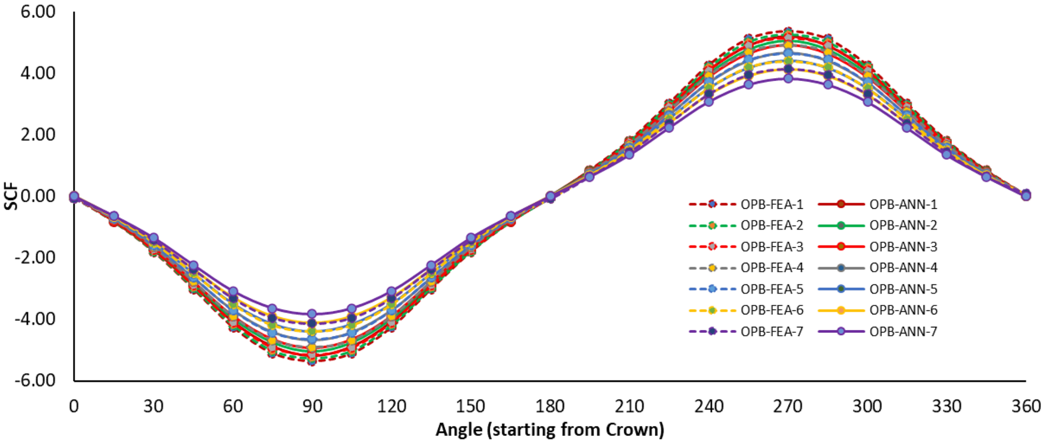

Figure 16. Comparison of SCF in KT-joint under OPB

The sign of SCF is dependent on the nature of the applied load. Axial tension results in positive SCF, while axial compression leads to negative SCF. IPB and OPB generate both tensile and compressive stress concentrations of equal magnitude, as depicted in Figures 15 and 16. The SCF sign must be maintained as it directly affects HSS. A more detailed discussion on this is available in Iqbal et al. [33]. The peak HSS is used for fatigue life assessment using the S-N curve. The empirical models developed for SCF estimation under uniplanar loads can be extended to estimate combined HSS for composite-reinforced KT-joints under multi-planar loading. By superimposing the HSS values obtained from uniplanar loads at 24 positions along the weld toe of the brace-chord interface, the combined HSS can be estimated. This combined HSS is used to determine the peak HSS, which, when used in conjunction with the S-N curve, allows for fatigue life estimation.

A MATLAB code was developed to automate this process. The code takes dimensionless parameters and loading information as inputs and outputs the HSS along the weld toe, including the peak HSS for use with the S-N curve. An example of the output plot generated by this code is shown in Figure 17. This plot illustrates the HSS distribution under 30 MPa axial tension, IPB, and OPB simulated loads, along with the combined HSS from their simultaneous effect. For individual axial compression and OPB, the peak HSS occurred at the crown, while for IPB, it was 15 degrees from the saddle point. When all three loads were applied simultaneously, forming a tri-planar loading condition, the peak HSS shifted to 288 degrees from the reference crown point. Additionally, the combined peak HSS magnitude was higher than that observed under individual loads, demonstrating the efficiency of the developed MATLAB code in estimating peak HSS rapidly and accurately.

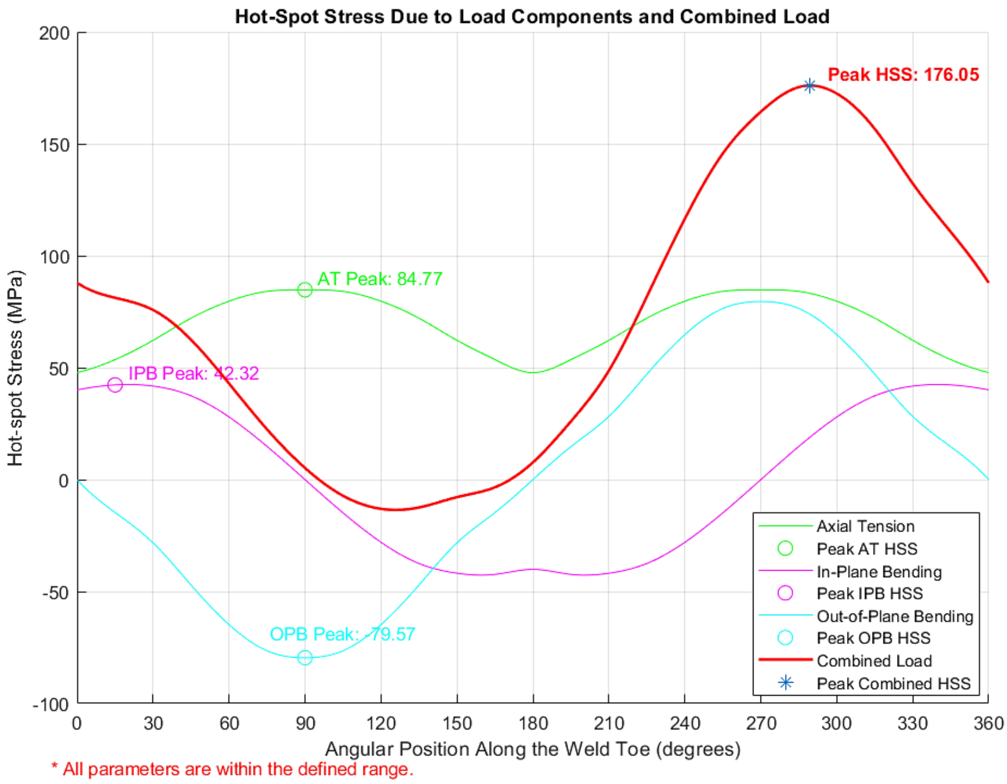

Figure 17. representative HSS plot for KT-joint under simultaneous axial, IPB, and OPB using the developed code

The only available published results for comparison were from Ahmadi & Zavvar [48], which included both simulation and experimental data for a KT-joint under axial compression, reporting a maximum difference of 15.9%, as shown in Figure 18. The results obtained from the developed FE model and ANN-based equations closely matched the FEA-based results of Ahmadi and Zavvar et al. [48], with a maximum percentage difference of 1.8% and 2.6%, respectively. The maximum difference between the developed models (FE and ANN-based) and experimental results was 16.2% and 16.8%, respectively. These discrepancies are likely due to unreported details in Ahmadi et al.'s experimental setup, such as dimensional precision and strain measurement techniques. Consequently, these differences are considered reasonable.

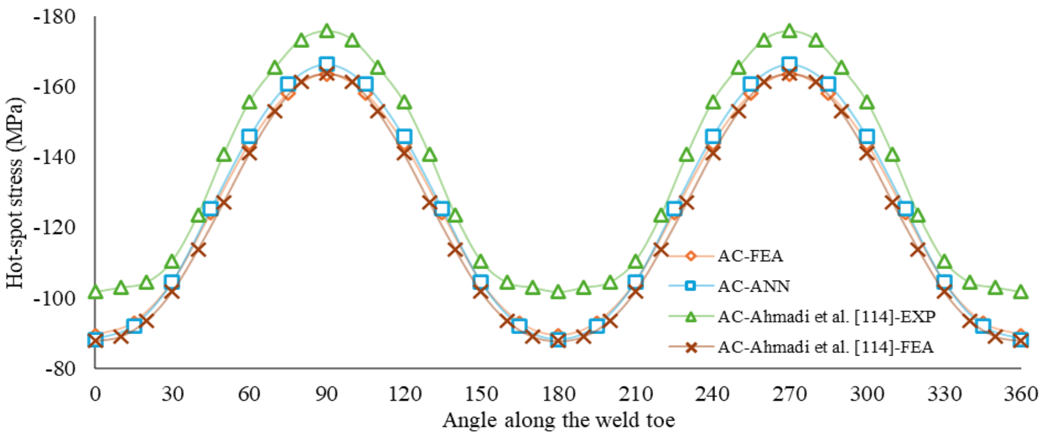

Figure 18. Validation of developed models through results of Ahmadi & Zavvar [48]

The experimental setup shown in Figure 19 was used to validate the surrogate model for axial compression. Figure 19-b presents the strain recorded from 48 strain gauges positioned at 24 stations along the weld toe, with two gauges per station used for linear extrapolation. Figure 19-b compares the SCF results. The maximum SCF difference obtained from the empirical model was approximately 15%, which falls below the 25% limit set by the UK Department of Energy and is thus deemed acceptable.

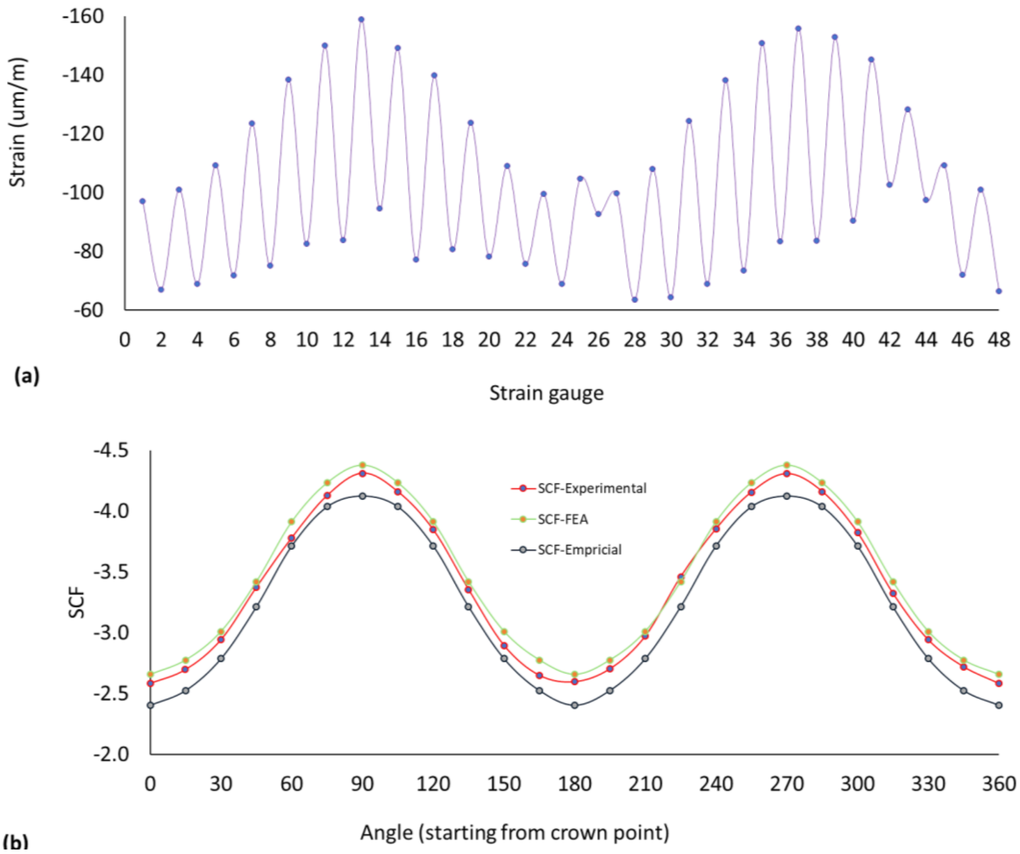

Figure 19. Validation of the empirical models (a) strain recorded (b) SCF comparison

4. Conclusion

This research investigated the reduction of stress concentration factors (SCFs) in composite-reinforced circular hollow section (CHS) KT-joints under multi-planar loading conditions using fiber-reinforced polymer (FRP) composites, an evolving rehabilitation technique. The application of FRP composites significantly reduced SCF, thereby enhancing fatigue life. The effectiveness of this reduction depended on the elastic modulus in the fiber direction, thickness, and orientation of the reinforcement. The optimal fiber orientation was found to be orthogonal to the weld toe. This can be achieved by wrapping the reinforcement around the brace while ensuring that the fibers remain orthogonal to the weld toe. Additionally, empirical models were developed to predict SCF in FRP-reinforced KT-joints. These models calculate SCFs at 24 positions along the weld toe, capturing the peak hot-spot stress (HSS) with a sensitivity of 15°. The peak HSS and the optimal reinforcement orientation were found to be coplanar. In combination with the principle of superposition, these models can determine both the location and magnitude of peak HSS as well as the optimal reinforcement orientation. The peak HSS obtained is then used in conjunction with the S-N curve for fatigue life estimation, similar to unreinforced tubular joints. The maximum difference in SCF between the developed models and finite element analysis (FEA) was found to be below 8%, while the difference between the developed models and experimental results was less than 15%. Future work includes further experimental validation.

5. Declarations

5.1. Author Contributions

Conceptualization, M.I. and S.K.; methodology, M.I.; software, M.I.; validation, M.I.; formal analysis, M.I.; investigation, M.I.; resources, S.K.; data curation, M.O.; writing—original draft preparation, M.I.; writing—review and editing, M.O. and V.P; visualization, M.I.; supervision, S.K. and V.P.; project administration, S.K.; funding acquisition, S.K. All authors have read and agreed to the published version of the manuscript.

5.2. Data Availability Statement

The data presented in this study are available on request from the corresponding author.

5.3. Funding

This research received funding from Yayasan Universiti Teknologi PETRONAS under Grant No. 015LC0-443.

5.4. Conflicts of Interest

The authors declare no conflict of interest.

6. References

[1] Nassiraei, H. (2025). Identification of the most suitable probability models for local joint flexibility in T/Y-connections stiffened with collar or doubler plates. Results in Engineering, 25, 104387. doi:10.1016/j.rineng.2025.104387.

[2] Yang, Y., Min, S., Peng, Y., Wang, H., & Chen, C. (2025). Experimental and numerical investigation on stress concentration factor of large-scale welded tubular T-joints. Ocean Engineering, 320, 120337. doi:10.1016/j.oceaneng.2025.120337.

[3] Zavvar, E., Rosa-Santos, P., Ghafoori, E., & Taveira-Pinto, F. (2025). Analysis of tubular joints in marine structures: A comprehensive review. Marine Structures, 99, 103702. doi:10.1016/j.marstruc.2024.103702.

[4] Iqbal, M., Karuppanan, S., Perumal, V., Ovinis, M., & Rasul, A. (2023). Rehabilitation Techniques for Offshore Tubular Joints. Journal of Marine Science and Engineering, 11(2), 461. doi:10.3390/jmse11020461.

[5] Iqbal, M., Karuppanan, S., Perumal, V., Ovinis, M., & Iqbal, M. (2024). A systematic review of stress concentration factors (SCFs) in composite reinforced circular hollow section (CHS) joints. Composites Part C: Open Access, 15, 100515. doi:10.1016/j.jcomc.2024.100515.

[6] ASME-PCC-2018. (2018). Repair of Pressure Equipment and Piping. The American Society of Mechanical Engineers, New York, United States.

[7] ISO 24817:2015. (2015). Petroleum, petrochemical and natural gas industries - Composite repairs for pipework - Qualification and design, installation, testing and inspection. International Organization for Standardization (ISO), Geneva, Switzerland.

[8] Zuo, G., Tong, L., Zhao, Z., Wang, H., Shi, W., & Yan, Y. (2025). SCF formulae of corrugated-web steel girders: Experiments and numerical analysis. Journal of Constructional Steel Research, 228, 109445. doi:10.1016/j.jcsr.2025.109445.

[9] Sadat Hosseini, A., Bahaari, M. R., & Lesani, M. (2019). Parametric Study of FRP Strengthening on Stress Concentration Factors in an Offshore Tubular T-Joint Subjected to In-Plane and Out-of-Plane Bending Moments. International Journal of Steel Structures, 19(6), 1755–1766. doi:10.1007/s13296-019-00244-0.

[10] Sadat Hosseini, A., Bahaari, M. R., & Lesani, M. (2019). Stress concentration factors in FRP-strengthened offshore steel tubular T-joints under various brace loadings. Structures, 20, 779–793. doi:10.1016/j.istruc.2019.07.004.

[11] Tong, L., Xu, G., Zhao, X. L., Zhou, H., & Xu, F. (2019). Experimental and theoretical studies on reducing hot spot stress on CHS gap K-joints with CFRP strengthening. Engineering Structures, 201, 296–313. doi:10.1016/j.engstruct.2019.109827.

[12] Xu, G., Tong, L., Zhao, X. L., Zhou, H., & Xu, F. (2020). Numerical analysis and formulae for SCF reduction coefficients of CFRP-strengthened CHS gap K-joints. Engineering Structures, 210, 369–86. doi:10.1016/j.engstruct.2020.110369.

[13] Sadat Hosseini, A., Bahaari, M. R., & Lesani, M. (2020). Experimental and parametric studies of SCFs in FRP strengthened tubular T-joints under axially loaded brace. Engineering Structures, 213, 110548. doi:10.1016/j.engstruct.2020.110548.

[14] Nassiraei, H., & Rezadoost, P. (2020). Stress concentration factors in tubular T/Y-joints strengthened with FRP subjected to compressive load in offshore structures. International Journal of Fatigue, 140, 105719. doi:10.1016/j.ijfatigue.2020.105719.

[15] Hosseini, A. S., Bahaari, M. R., & Lesani, M. (2020). SCF distribution in FRP-strengthened tubular T-joints under brace axial loading. Scientia Iranica, 27(3 A), 1113–1129. doi:10.24200/SCI.2018.5471.1293.

[16] Nassiraei, H., & Rezadoost, P. (2021). Stress concentration factors in tubular T/Y-connections reinforced with FRP under in-plane bending load. Marine Structures, 76, 102871. doi:10.1016/j.marstruc.2020.102871.

[17] Nassiraei, H., & Rezadoost, P. (2021). Parametric study and formula for SCFs of FRP-strengthened CHS T/Y-joints under out-of-plane bending load. Ocean Engineering, 221, 108313. doi:10.1016/j.oceaneng.2020.108313.

[18] Sadat Hosseini, A., Zavvar, E., & Ahmadi, H. (2021). Stress concentration factors in FRP-strengthened steel tubular KT-joints. Applied Ocean Research, 108, 1187–221. doi:10.1016/j.apor.2021.102525.

[19] Nassiraei, H., & Rezadoost, P. (2021). SCFs in tubular X-joints retrofitted with FRP under out-of-plane bending moment. Marine Structures, 79, 103010. doi:10.1016/j.marstruc.2021.103010.

[20] Nassiraei, H., & Rezadoost, P. (2021). SCFs in tubular X-connections retrofitted with FRP under in-plane bending load. Composite Structures, 274, 114314. doi:10.1016/j.compstruct.2021.114314.

[21] Zavvar, E., Sadat Hosseini, A., & Lotfollahi-Yaghin, M. A. (2021). Stress concentration factors in steel tubular KT-connections with FRP-Wrapping under bending moments. Structures, 33, 4743–4765. doi:10.1016/j.istruc.2021.06.100.

[22] Nassiraei, H., & Rezadoost, P. (2022). Development of a probability distribution model for the SCFs in tubular X-connections retrofitted with FRP. Structures, 36, 233–247. doi:10.1016/j.istruc.2021.10.033.

[23] Xu, X., Shao, Y., Gao, X., & Mohamed, H. S. (2022). Stress concentration factor (SCF) of CHS gap TT-joints reinforced with CFRP. Ocean Engineering, 247, 110722. doi:10.1016/j.oceaneng.2022.110722.

[24] Mohamed, H. S., Zhang, L., Shao, Y. B., Yang, X. S., Shaheen, M. A., & Suleiman, M. F. (2022). Stress concentration factors of CFRP-reinforced tubular K-joints via Zero Point Structural Stress Approach. Marine Structures, 84, 103239. doi:10.1016/j.marstruc.2022.103239.

[25] Mohamed, H. S., Yang, X. S., Shao, Y. B., Shaheen, M. A., Suleiman, M. F., Zhang, L., & Hossian, A. (2022). Stress concentration factors (SCF) of CFRP-reinforced T/Y-joints via ZPSS approach. Ocean Engineering, 261, 112092. doi:10.1016/j.oceaneng.2022.112092.

[26] Sadat Hosseini, A., Bahaari, M. R., & Lesani, M. (2022). Formulas for Stress Concentration Factors in T&Y Steel Tubular Joints Stiffened with FRP under Bending Moments. International Journal of Steel Structures, 22(5), 1408–1432. doi:10.1007/s13296-022-00651-w.

[27] Zavvar, E., Henneberg, J., & Guedes Soares, C. (2023). Stress concentration factors in FRP-reinforced tubular DKT joints under axial loads. Marine Structures, 90, 429–52. doi:10.1016/j.marstruc.2023.103429.

[28] Mohamed, H. S., Yang, X. S., Liao, F. Y., & Fu, T. (2024). SCF determination of the CFRP- fortified T/Y-joints exposed to IPB or OPB moment via ZPSS approach. Structures, 61. doi:10.1016/j.istruc.2024.105997.

[29] Rashnooie, R., Zeinoddini, M., Ghafoori, E., & Sharafi, M. (2024). Experimental and numerical study on the in-plane bending behaviour of FRP-strengthened steel tubular welded T-joints. Thin-Walled Structures, 201, 112000. doi:10.1016/j.tws.2024.112000.

[30] Zavvar, E., Sousa, F., Giannini, G., Taveira-Pinto, F., & Santos, P. R. (2024). Probability of maximum values of stress concentration factors in tubular DKT-joints reinforced with FRP under axial loads. Structures, 66, 106809. doi:10.1016/j.istruc.2024.106809.

[31] Zavvar, E., Sousa, F., Taveira-Pinto, F., & Rosa Santos, P. (2024). Multivariate Data Analysis of Maximum Stress Concentration Factors in FRP-Retrofitted Two-Planar KT-Joints under Axial Loads for Offshore Renewables. Journal of Marine Science and Engineering, 12(8), 1451. doi:10.3390/jmse12081451.

[32] Rezadoost, P., & Nassiraei, H. (2024). Best Probability Distribution for SCFs in FRP-Strengthened T/Y-Shaped Connections under Out-of-Plane Bending Loading. 21-22 May, 2024, University of Zanjan, Zanjan, Iran.

[33] Iqbal, M., Karuppanan, S., Perumal, V., Ovinis, M., & Nouman, H. (2023). Empirical modeling of stress concentration factors using finite element analysis and artificial neural networks for the fatigue design of tubular KT-joints under combined loading. Fatigue and Fracture of Engineering Materials and Structures, 46(11), 4333–4349. doi:10.1111/ffe.14122.

[34] Ahmadi, H., Lotfollahi-Yaghin, M. A., & Aminfar, M. H. (2011). Effect of stress concentration factors on the structural integrity assessment of multi-planar offshore tubular DKT-joints based on the fracture mechanics fatigue reliability approach. Ocean Engineering, 38(17–18), 1883–1893. doi:10.1016/j.oceaneng.2011.08.004.

[35] Sadat Hosseini, A., Bahaari, M. R., Lesani, M., & Hajikarimi, P. (2021). Static load-bearing capacity formulation for steel tubular T/Y-joints strengthened with GFRP and CFRP. Composite Structures, 268, 263–81. doi:10.1016/j.compstruct.2021.113950.

[36] Moffat, D. G., Kruzelecki, J., & Blachut, J. (1996). The Effects of Chord Length and Boundary Conditions on the Static Strength of a Tubular T-Joint under Brace Compression Loading. Marine Structures, 9(10), 935–947. doi:10.1016/0951-8339(96)00007-X.

[37] Smedley, P., & Fisher, P. (1991). Stress concentration factors for simple tubular joints. Health and Safety Executive - Offshore Technology Report.

[38] ARSEM. (1987). Design Guides for Offshore Structures, Volume 1 - Welded Tubular Joints. Association de Recherche sur les Structures Métalliques Marines (ARSEM), Paris, France.

[39] API (2014). Recommended Practice for Planning, D. and C.F.O.P.-W.S.D. (2014). API RP 2A WSD 22nd Edition, vol. 2014. American Petroleum Institute (API), Washington, United States.

[40] Ahmadi, H., & Nejad, A. Z. (2016). Stress concentration factors in uniplanar tubular KT-joints of jacket structures subjected to in-plane bending loads. International Journal of Maritime Technology, 5, 27-39.

[41] Ahmadi, H. (2019). Probabilistic analysis of the DoB in axially-loaded tubular KT-joints of offshore structures. Applied Ocean Research, 87, 64–80. doi:10.1016/j.apor.2019.03.018.

[42] Ahmadi, H., & Lotfollahi-Yaghin, M. A. (2013). Experimental and numerical investigation of geometric SCFs in internally ring-stiffened tubular KT-joints of offshore structures. Journal of the Persian Gulf, 4(12), 1-12.

[43] Ahmadi, H., & Zavvar, E. (2015). Stress concentration factors induced by out-of-plane bending loads in ring-stiffened tubular KT-joints of jacket structures. Thin-Walled Structures, 91, 82–95. doi:10.1016/j.tws.2015.02.011.

[44] Zhang, Y., Zhang, K., Zhao, H., Xin, J., & Duan, M. (2018). Stress analysis of adhesive in a cracked steel plate repaired with CFRP. Journal of Constructional Steel Research, 145, 210–217. doi:10.1016/j.jcsr.2018.02.029.

[45] Ullah, H., Harland, A. R., & Silberschmidt, V. V. (2012). Experimental and numerical analysis of damage in woven GFRP composites under large-deflection bending. Applied Composite Materials, 19(5), 769–783. doi:10.1007/s10443-011-9242-7.

[46] Ganesh, V. K., & Naik, N. K. (1993). Some strength studies on FRP laminates. Composite Structures, 24(1), 51–58. doi:10.1016/0263-8223(93)90054-T.

[47] Iqbal, M., Karuppanan, S., Perumal, V., Ovinis, M., & Khan, A. (2025). Stress Concentration Factors in CFRP-Reinforced KT-Joints under Multiplanar Bending Loads: Experimental and Numerical Investigation. Results in Engineering, 25(103745), 103745. doi:10.1016/j.rineng.2024.103745.

[48] Ahmadi, H., & Zavvar, E. (2020). Degree of bending (DoB) in offshore tubular KT-joints under the axial, in-plane bending (IPB), and out-of-plane bending (OPB) loads. Applied Ocean Research, 95, 1187–206. doi:10.1016/j.apor.2019.102015.

[49] Ahmadi, H., Yeganeh, A., Mohammadi, A. H., & Zavvar, E. (2016). Probabilistic analysis of stress concentration factors in tubular KT-joints reinforced with internal ring stiffeners under in-plane bending loads. Thin-Walled Structures, 99, 58–75. doi:10.1016/j.tws.2015.11.010.

[50] Hobbacher, A. (1996). Fatigue Design of Welded Joints and Components. Recommendations of IIW Joint Working Group XIII-1539–96/XV-845–96, The International Institute of Welding, Genoa, Italy.

[51] Gurney, T. R. (1991). The Fatigue Strength of Transverse Fillet Welded Joints. The Fatigue Strength of Transverse Fillet Welded Joints, Abington Publishing, Parks Blvd Nashville, United States. doi:10.1533/9780857093257.

[52] Poutiainen, I., Tanskanen, P., & Marquis, G. (2004). Finite element methods for structural hot spot stress determination - A comparison of procedures. International Journal of Fatigue, 26(11), 1147–1157. doi:10.1016/j.ijfatigue.2004.04.003.

[53] Radaj, D., Sonsino, C., & Fricke, W. (2006). Fatigue assessment of welded joints by local approaches, Second Edition. CRC Press, Boca Raton, United States. doi:10.1201/9781439832806.

[54] Maddox, S. J. (2002). Fatigue Strength of Welded Structures. In Fatigue Strength of Welded Structures. Woodhead Publishing, Sawston, United Kingdom. doi:10.1016/c2013-0-17455-7.

[55] Manson, S. S. (1965). Fatigue: A Complex Subject-Some Simple Approximations some approximations useful in design are outlined and their application illustrated. Experimental Mechanics, 5(4), 193–226.

[56] Niemi, E., Fricke, W., & Maddox, S. J. (2018). The Structural Hot-Spot Stress Approach to Fatigue Analysis. In: Structural Hot-Spot Stress Approach to Fatigue Analysis of Welded Components. IIW Collection, Springer, Singapore. doi:10.1007/978-981-10-5568-3_2.

[57] Hobbacher, A. F. (2017). Erratum to: Recommendations for Fatigue Design of Welded Joints and Components. Recommendations for Fatigue Design of Welded Joints and Components, E1–E1, Springer, Cham, Switzerland. doi:10.1007/978-3-319-23757-2_7.

[58] Lesani, M., Bahaari, M. R., & Shokrieh, M. M. (2015). FRP wrapping for the rehabilitation of Circular Hollow Section (CHS) tubular steel connections. Thin-Walled Structures, 90, 216–234. doi:10.1016/j.tws.2014.12.013.

[59] Hawileh, R. A., Musto, H. A., Abdalla, J. A., & Naser, M. Z. (2019). Finite element modeling of reinforced concrete beams externally strengthened in flexure with side-bonded FRP laminates. Composites Part B: Engineering, 173, 106952. doi:10.1016/j.compositesb.2019.106952.

[60] Fu, Y., Tong, L., He, L., & Zhao, X. L. (2016). Experimental and numerical investigation on behavior of CFRP-strengthened circular hollow section gap K-joints. Thin-Walled Structures, 102, 80–97. doi:10.1016/j.tws.2016.01.020.

[61] Efthymiou, M. (1988). Development of SCF formulae and generalized influence functions for use in fatigue analysis. OTJ 88. Recent Developments in Tubular Joints Technology, 4-5 October, 1988, Surrey, United Kingdom.

[62] N'Diaye, A., Hariri, S., Pluvinage, G., & Azari, Z. (2007). Stress concentration factor analysis for notched welded tubular T-joints. International Journal of Fatigue, 29(8), 1554–1570. doi:10.1016/j.ijfatigue.2006.10.030.

[63] Ahmadi, H., Lotfollahi-Yaghin, M. A., & Yong-Bo, S. (2013). Chord-side SCF distribution of central brace in internally ring-stiffened tubular KT-joints: A geometrically parametric study. Thin-Walled Structures, 70, 93–105. doi:10.1016/j.tws.2013.04.011.

[64] Mohammed, A., Dasari, S. R., Khandelwal, S. K., & Desai, Y. M. (2024). Advancements in stress concentration factor computation for tubular X joints through Bayesian-optimized neural networks. Structures, 67, 106962. doi:10.1016/j.istruc.2024.106962.

[65] Iqbal, M., Karuppanan, S., Perumal, V., Ovinis, M., Iqbal, M., & Rasul, A. (2024). Optimization of fibre orientation for composite reinforcement of circular hollow section KT-joints. International Journal of Structural Integrity, 15(4), 717–730. doi:10.1108/IJSI-04-2024-0054.